Dynamics of particle production in Pb-Pb collisions at $\sqrt{s_{NN}} = 2.76$ TeV using the PYTHIA8 Angantyr model

Ravindra Singh,* Yoshini Bailung, and Ankhi Roy
Discipline of Physics, Indian Institute of Technology Indore, Simrol, Indore 453552, India

(Received 2 August 2021; revised 29 November 2021; accepted 22 February 2022; published 4 March 2022)

We study the dynamics of identified, strange, and multistrange particle production in Pb-Pb collisions at $\sqrt{s_{NN}} = 2.76$ TeV using the recently developed Angantyr model, incorporated within PYTHIA8. We show the interplay between multiparton interactions (MPIs) and color reconnection (CR) on the experimentally measured quantities. We also investigate the role of string shoving within the rope hadronization framework and its impact in particle production. The charged-particle multiplicity (N_{ch}) and mean transverse momentum ($\langle p_{\mathrm{T}} \rangle$) distributions are well explained by PYTHIA8 Angantyr with proper tuning, as presented in this paper. Predictions of p_{T} spectra, $\langle p_{\mathrm{T}} \rangle$, and p_{T} integrated yields of the identified, strange, and multistrange particles are studied. To provide insight into the collective nature of the produced particles, we look into the ratio of particle yields to pions and kaons. PYTHIA8 Angantyr with MPI+CR and hadronization via string shoving is seen to mimic signs of collectivity due to different implementations in string interactions.

DOI: 10.1103/PhysRevC.105.035202

I. INTRODUCTION

The study of how matter behaves at extreme temperature and energy densities is vital to understand the nature of phase transition in quantum chromodynamics (QCD) [1–3]. Facilities like the Relativistic Heavy Ion Collider (RHIC) at BNL, USA, and the Large Hadron Collider (LHC) at CERN, Geneva, Switzerland, are of prime importance to unravel the properties of the produced hot QCD matter [4–7]. A deconfined state of quarks and gluons, also known as quark-gluon plasma (QGP), is believed to be created for a very short time in these heavy-ion collisions experiments. In this QGP phase, the relevant degrees of freedom are quarks and gluons rather than mesons and baryons, confined to color-neutral states [4,8,9].

An initial and important observable is the multiplicity distribution ($dN_{\mathrm{ch}}/d\eta$) of the charged particles, which is essential to extract the properties of produced particles and their interactions [7]. Such distributions in a particular pseudorapidity range were measured in the CERN proton-antiproton ($p\bar{p}$) collider experiments in the 1980s [10–13]. These measurements provide information on the energy density and centrality of the colliding system. The centrality is directly related to the initial overlap region geometry, which corresponds to the number of participating nucleons and binary collisions [14].

For the final-state charged particles, the rapidity (y) or pseudorapidity (η) and transverse momentum (p_{T}) spectra are known to reflect the degrees of longitudinal extension and transverse excitation of the interacting system, respectively [15,16]. Distributions in low p_{T} ranges let us inspect the transverse excitation and soft processes, whereas higher p_{T} corresponds to hard scattering processes. In low energy collisions, one can neglect hard processes, as most of the contribution comes from soft processes. At high center-of-mass energies, hard processes have finite contribution albeit the soft processes are predominant [17]. From the final state charged particle p_{T} spectra, one can extract information about the thermal nature of the interacting system [18,19], and can comment on the formation and characteristic properties of the formed matter. According to the Maxwell-Boltzmann distribution law, the p_{T} spectra are related to the temperature of the system formed in these collisions. The N_{ch} of charged particles formed in ultrarelativistic collisions also depends on the system's temperature and density. Since most of the final state charged particles are part of a locally thermalized medium, the mean transverse momentum $\langle p_{\mathrm{T}} \rangle$ distribution vs N_{ch} is expected to be more or less flat in heavy-ion systems like Pb-Pb at high N_{ch}. The contributions at lower N_{ch} are mostly from the peripheral collisions where a QGP is less likely to be produced.

The ratios of yields of identified hadrons are important to understand to the mechanism of hadron production. The ratios of proton to pion (p/π) and kaon to pion (K/π) characterize the relative baryon and meson production, respectively. Additionally, K/π, Λ/π, Σ^0/π, Ξ^0/π, and Ω/π ratios represent the strangeness production at higher multiplicities, indicating a universal underlying dynamics in hadron production for different quark-gluon final states. Strangeness enhancement is proposed as a signature of QGP formation in heavy-ion collisions [20–22] because of the faster equilibration of strangeness production processes in a QGP than any other process in a hadron gas [23,24]. This is observed to be more prominent for multistrange hadrons [25]. The production mechanism of strange hadrons provides a way to investigate the properties of the hot QCD matter.

Another essential medium characteristic is anisotropic flow, considered the proof of collective behavior of partons and hadrons [26–28]. In a heavy-ion collision, the

*ravirathore.physics@gmail.com

TABLE I. Centrality classes and the corresponding charged particle multiplicities (N_{ch}) in PYTHIA8 Angantyr with MPI+CR and string shoving.

Serial No.	Centrality (%)	MPI+CR	Shoving
I	0–5	2314–3050	2117–2900
II	5–10	1947–2314	1782–2117
III	10–20	1387–1947	1270–1782
IV	20–30	967–1387	885–1270
V	30–40	644–967	590–885
VI	40–50	399–644	367–590
VII	50–60	224–399	205–367
VIII	60–70	108–224	99–205
IX	70–80	43–108	39–99

hydrodynamic expansion is a consequence of the transverse pressure gradient. This transverse flow shifts the produced particles to higher momenta, and, due to higher gain in momenta of heavy particles from flow velocity, the increment is more for heavier particles. This effect is seen commonly for heavy-ion systems and even high multiplicity *pp* and *p*-Pb collisions [25].

In this work, we have explored all the above-mentioned aspects of particle production in Pb-Pb collisions at $\sqrt{s_{NN}} =$ 2.76 TeV using the Angantyr model, which is the heavy-ion extension of the PYTHIA8, extensively used for *pp* collisions. The paper is organized as follows: In Sec. II, the details of event generation and analysis methodology are discussed. Section III presents the results and discussions. Finally, in Sec. IV, we summarize our findings.

II. EVENT GENERATION AND ANALYSIS METHODOLOGY

PYTHIA is an event generator that is extensively and successfully used for the study of proton-proton and proton-lepton collisions. Recent advancement in PYTHIA8 enables the study of heavy nuclei collisions, namely proton-nuclei (*pA*) and nuclei-nuclei (*AA*). In this work, the PYTHIA8 event generator is used to simulate ultrarelativistic Pb-Pb collisions with Angantyr [29]. PYTHIA8 natively does not support heavy-ion systems; however, the Angantyr model combines several nucleon-nucleon collisions into one heavy-ion collision. It is a combination of many-body physics (theoretical) models suitable for producing hard and soft interactions, initial and final-state parton showers, particle fragmentation, multipartonic interactions, color reconnection mechanisms, and decay topologies [30]. In this study, we use PYTHIA8 [31] which includes multiparton interactions (MPIs), color reconnection (CR), and rope hadronization mechanisms in particle production. MPI is vital to expostulate the underlying events, multiplicity distributions, and charmonia production. In general, an event generator at high colliding energies produces around four to ten partonic interactions, which depend on the overlapping region of colliding particles [32]. The perturbative scattering processes are implemented by initial state radiation (ISR) and final state radiation (FSR) [33,34].

Hadronization in PYTHIA8 is done using the Lund string fragmentation model [35]. The beam remnants and the produced partons are interconnected via strings storing potential energy. The string interactions in PYTHIA8 can be carried out in coordinate and color space via ropes, color reconnection, and string shoving mechanisms. The mode of interaction between the strings govern the hadronization mechanism. These

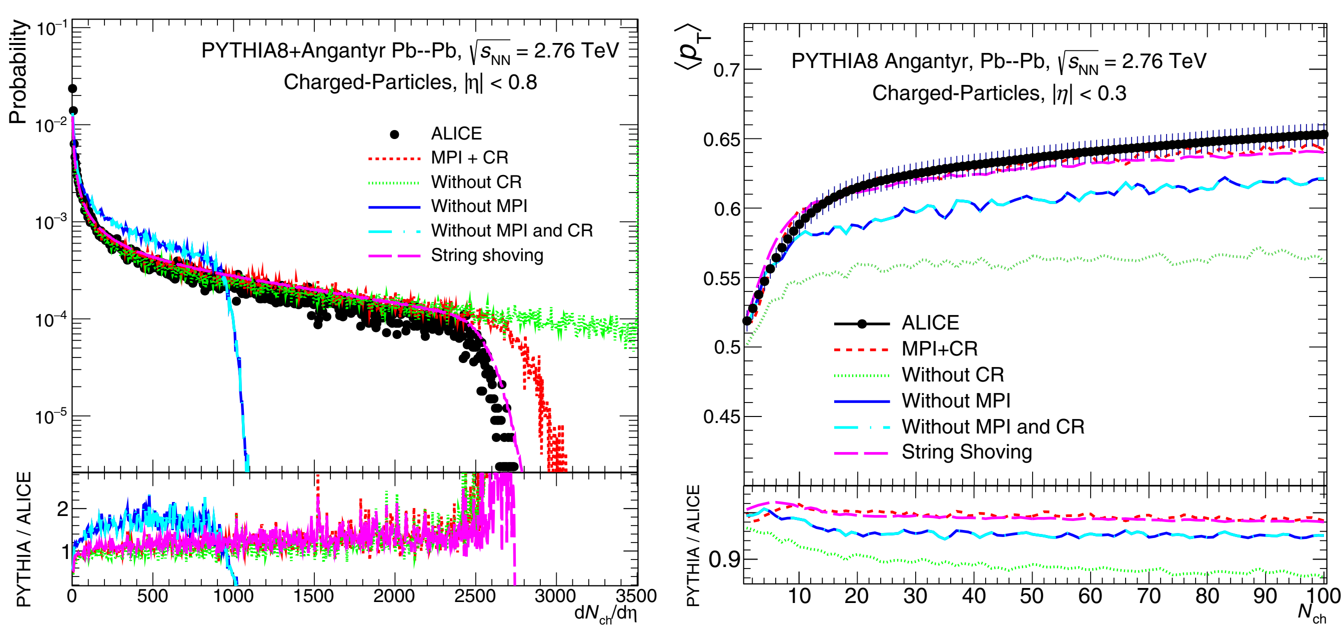

FIG. 1. Left: Multiplicity distribution of charged particles from PYTHIA8 Angantyr with different tunes and ALICE data. Right: $\langle p_T \rangle$ distribution vs charged-particle multiplicity in different PYTHIA8 tunes and ALICE data. The lower panels show the ratio of PYTHIA8 Angantyr predictions over data for the different configurations considered.

TABLE II. Mean and RMS of charge particle multiplicity in different PYTHIA8 tunes.

	MPI+CR	CR off	MPI off	(MPI+CR) off	Shoving
Mean	704.1	882.8	276.6	276.6	647.6
RMS	759.5	961.2	274.3	274.3	697.8

underlying mechanisms are responsible for the signatures in heavy-ion measurements without any thermalized medium within PYTHIA8. The rope hadronization model allow strings to overlap in transverse space to create a "rope." Within these overlapping strings in the impact parameter space, the energy density between the region of overlap and outside, creates a pressure gradient which pushes the strings outside. This mechanism in PYTHIA8 is accomplished by making the strings "shove" each other apart. String shoving in PYTHIA8 Angantyr influences the ratio to strange and nonstrange hadrons, which can explain the strangeness enhancement in *pp* and heavy ion measurements. In the CR mechanism, color strings are effectively shorter. This leads to decrease in particle production and consequently the multiplicity ($N_{\rm ch}$). This is compensated by the addition of MPI as a parton level phenomenon in PYTHIA8 which increases particle production. In contrast, strings are effectively longer in string shoving, which leads to increase in particle production. In literature, flowlike effects in *pp* collisions are well mimicked by string shoving and CR mechanisms [36] in PYTHIA8.

In Angantyr, positions and the number of the interacting nucleons and binary nucleon-nucleon collisions are performed by Glauber-model-based eikonal approximation in impact-parameter space. Furthermore, Gribov's corrections are implemented in order to include diffractive excitation, which appears due to the fluctuations in the nucleon substructure. Angantyr is the first model which implements diffractive excitation in both projectile and target nuclei via individual fluctuations. This is essential to generalize for an *AA* system [29]. The contribution to the final state from each participating nucleon is induced from the Fritiof model with the concept of wounded nucleons (diffractive and nondiffractive). The hard partonic subcollisions, normalized by nucleon-nucleon subcollisions, play a crucial role at high energies. The model treats the projectile and target nucleons via two interaction scenarios. In one case, the interactions between the species are considered as *pp*-like nondiffractive (ND) processes. This is entirely driven by PYTHIA8. However, in the second scenario, a wounded projectile nucleon can have ND interactions with many target nucleons, which are termed secondary ND (SD) collisions. Subevents are generated solely through PYTHIA8, where these SD collisions are put into play as modified SD processes [37]. Depending on the interaction probability, interactions between wounded nucleons are classified as elastic, nondiffractive, secondary nondiffractive, single diffractive, and double-diffractive.

We have generated around 2×10^6 events in Pb-Pb at $\sqrt{s_{NN}} = 2.76$ TeV. The inelastic, nondiffractive component of the total crosssection for all soft QCD processes is used with the switch `SoftQCD:all = on` with the MPI based scheme

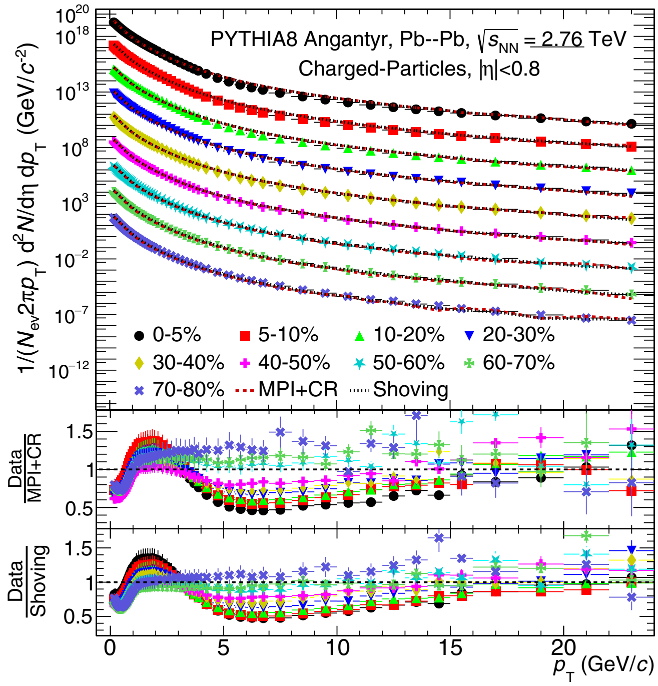

FIG. 2. Charged-particle $p_{\rm T}$ spectra in nine centrality classes described in Table I from PYTHIA8 Angantyr and ALICE data. The middle and lower panels represent the deviation of PYTHIA8 Angantyr predictions from MPI+CR and string shoving respectively with data.

of color reconnection (`ColorReconnection:mode(0)`). For string shoving, under the rope hadronization framework (`Ropewalk:RopeHadronization = on`), we switch string shoving via `Ropewalk:doShoving = on` and turn off flavor ropes by `Ropewalk:doFlavour = off`. The classes based on charged particle multiplicities ($N_{\rm ch}$) have been chosen within the pseudorapidity window of $-0.8 < \eta < 0.8$ to match the acceptance of the Time Projection Chamber (TPC) detector in ALICE [27]. The events generated using these cuts are divided into nine multiplicity classes, each class containing 10% of total events except the first two classes which contain 5% of total events as used in [27]. The $N_{\rm ch}$ classes corresponding to different centralities are tabulated in Table I. Heavy strange particles are chosen from their specific decay channels and Particle Data Group codes.

III. RESULTS AND DISCUSSION

The charged-particle multiplicity distributions for different PYTHIA8 tunes within $|\eta| < 0.8$ are shown in the Fig. 1. To see the effect of different PYTHIA tunes, we consider the following configurations: MPI with/without CR, no MPI, and both MPI and CR off and string shoving. It is observed that results from MPI+CR and string shoving tunes are compatible with ALICE data. MPI without CR overestimates, whereas the tune without MPI is seen to underestimate our results. We also observe that there is no effect of CR if MPI is off. The particle production increases with MPI, due to interpartonic interactions; on the other hand, while turning CR off, particle

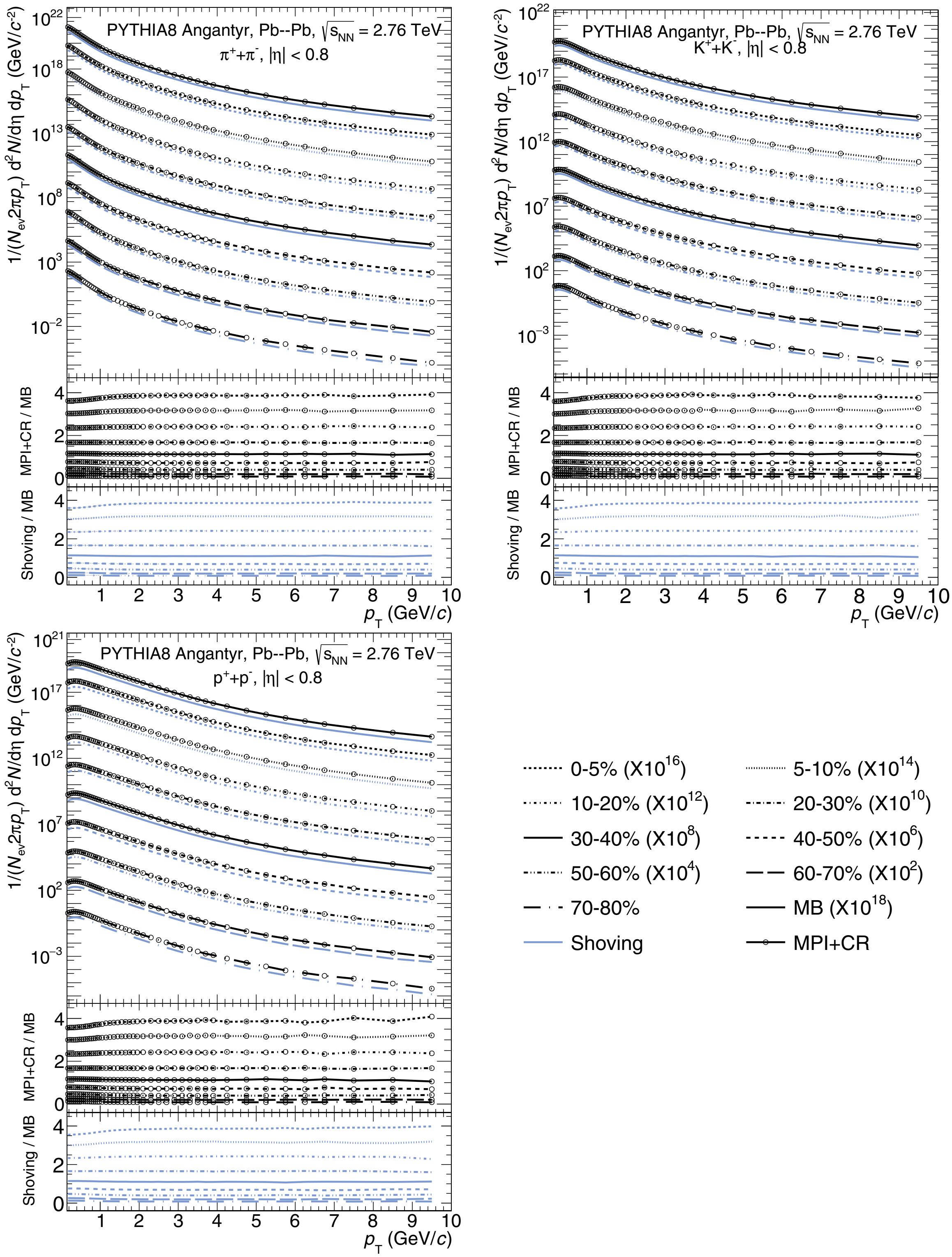

FIG. 3. p_T spectra of identified charged particles [$\pi^{\pm}$, $K^{\pm}$, $p(\bar{p})$] in various centrality classes. The middle and lower panels show the ratios for each centrality class to MB for MPI+CR and string shoving respectively.

production increases. In the color reconnection (CR) scheme, the string lengths are reduced; in consequence, when CR is kept on, particle production lessens [36]. Turning MPI off removes the strings between the partons. As a result, we do not observe any effect of CR. String shoving shows the best agreement with the data amongst all the tunes. The fragmentation of longer strings lead to higher particle production. To quantify the effect of the tunes used, the mean and RMS of the multiplicity distributions are measured and reported in Table II. The mean for MPI+CR is around 2.5 times larger

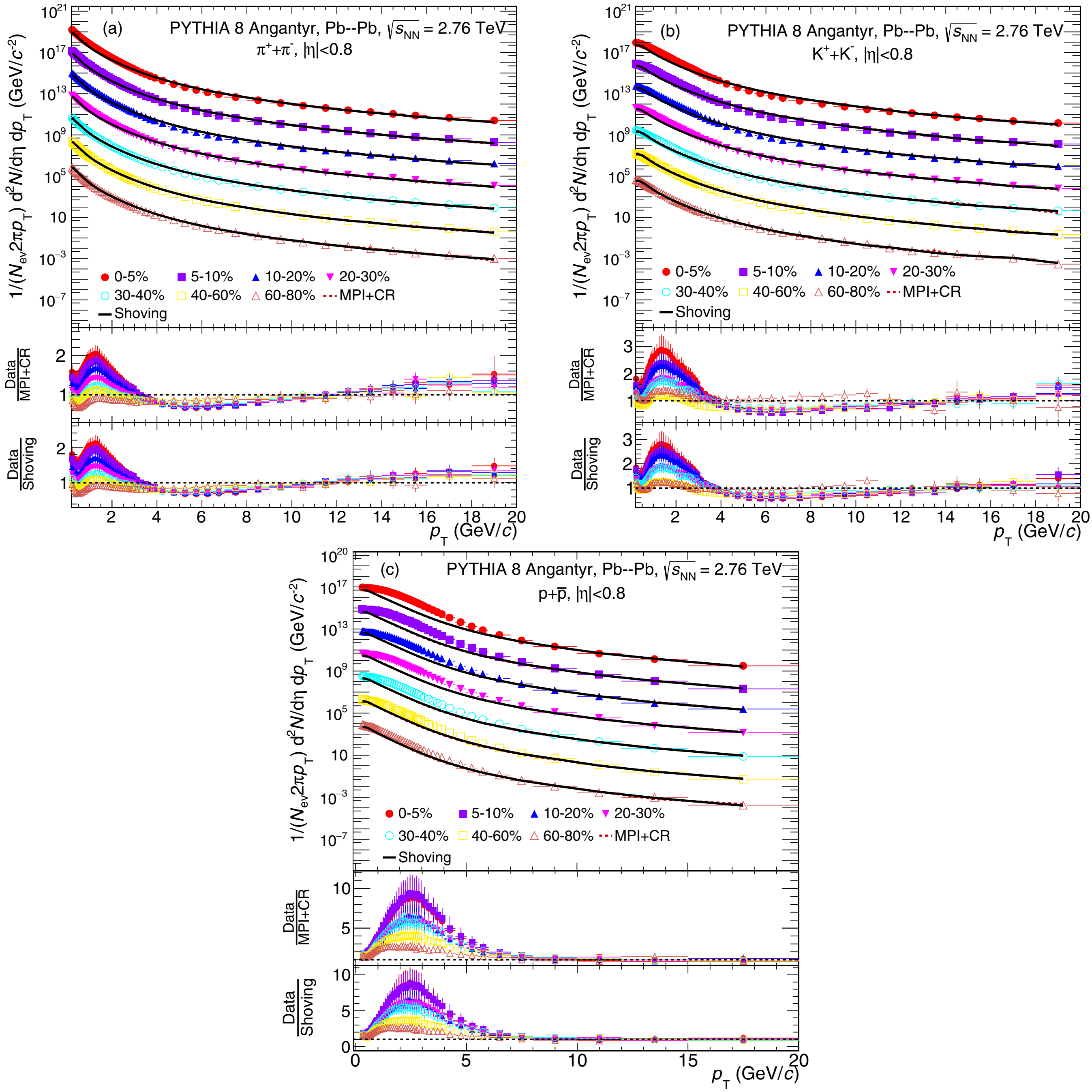

FIG. 4. p_{T} spectra of identified charged particles [$\pi^{\pm}$, $K^{\pm}$, $p(\bar{p})$]. The middle and lower panels show the ratios for different centrality classes to data with MPI+CR and string shoving.

without MPI and around 3.2 times larger without CR compared without MPI. A similar comparison can be made for the RMS values between these settings. For MPI+CR turned off, we report similar values for mean and RMS, which confirms our statement made earlier. The results from string shoving are closer than any other tune to ALICE data. This is accredited to the higher effective length of the color ropes, leading to higher particle production via fragmentation.

By observing different tunes in Fig. 1 (left), we can conclude that inclusion of hadronization via MPI+CR mode and via string shoving which is a part of the rope hadronization framework, are favorable settings to describe ALICE data [27]. We also observed similar results after comparing the $\langle p_{\mathrm{T}} \rangle$ distribution as a function of charged-particle multiplicity using simulated PYTHIA8 Angantyr and experimental data as shown in Fig. 1 (right). Distributions obtained from PYTHIA8 are scaled with a constant (1.138) factor for better visualization and to compare the slope of different distributions with data [38]. The $\langle p_{\mathrm{T}} \rangle$ distributions with MPI+CR and string shoving describe the data very well, even without hydrody-

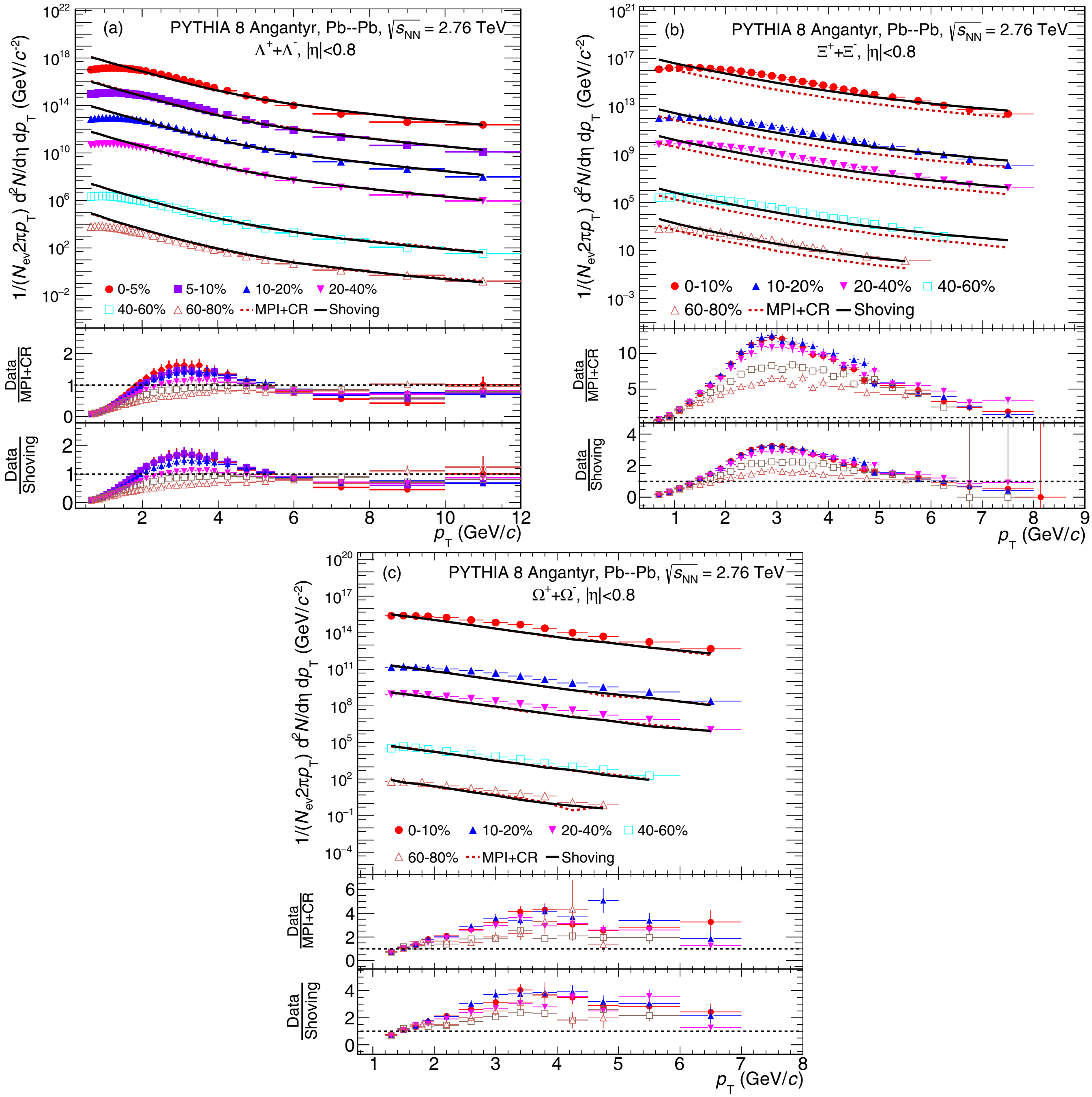

FIG. 5. p_T spectra of strange and multistrange baryons ($\Lambda^{\pm}$, $\Xi^{\pm}$, $\Omega^{\pm}$). The middle and lower panels show the ratios for different centrality classes to data with MPI+CR and string shoving.

namics. $\langle p_T \rangle$ with MPI off (or MPI and CR off) describes data below $N_{ch} = 10$ very well but deviates at higher values, becoming almost flat at high multiplicities. This is probably due to the large production of low multiplicity events when MPI is kept off. A similar trend is seen for CR turned off; however, the ratio of $\langle p_T \rangle$ over data decreases as we go to higher values in multiplicity, as reconnection occurs in such a way that the strings between partons are as small as possible. This attribute is credited to CR, where a correlation between N_{ch} and $\langle p_T \rangle$ can be seen [39]. Preceding hadronization, strings fuse to form high p_T hadrons. With CR off, fewer strings fuse to form hadrons during hard scatterings, explaining the increment of $\langle p_T \rangle$ at higher multiplicities. For hadronization via string shoving, the trend for $\langle p_T \rangle$ is very close to the MPI+CR tune, describing the data very well. We conclude that MPI+CR and string shoving frameworks have similar outcomes when it comes to particle production.

To further check the compatibility of simulated data, we compare the p_T spectra of final state charged particles with ALICE measurements in different centrality classes within experimental kinematic selections, which is shown in Fig. 2. The p_T spectra of each centrality class are scaled to the slope

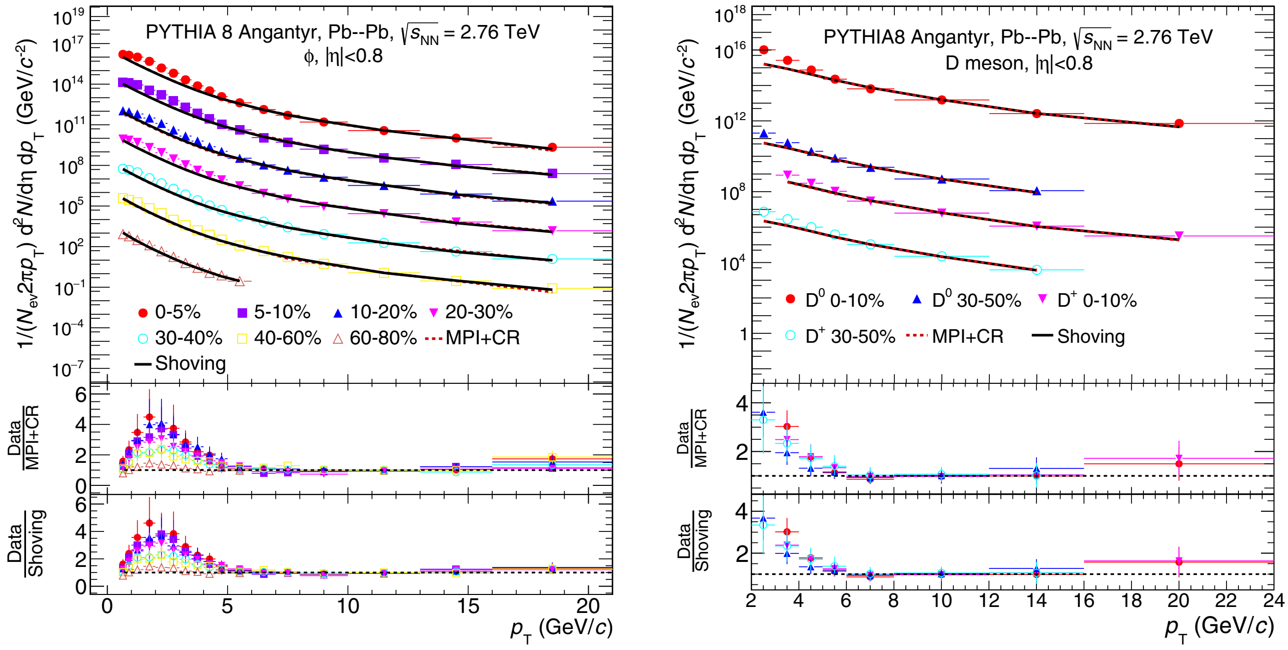

FIG. 6. p_T spectra of ϕ and D mesons. The middle and lower panels show the ratios for each centrality class to data with MPI+CR and string shoving.

with ALICE measurements for clearer visualization and comparison. From the lower panels of Fig. 2, it is observed that the experimental and simulated data are comparable within statistical uncertainties.

With the assurance of the quality of the simulated data discussed above, we now move on to study the transverse momentum spectra of identified particles, p_T integrated yield of identified and strange particles, and particle ratios with PYTHIA8 Angantyr.

A. Transverse momentum spectra of identified particles

Figure 3 shows the p_T spectra of identified charge-particles $\pi^{\pm}$, $K^{\pm}$, and $p(\bar{p})$ in different centrality classes and for minimum bias (MB). The spectra were obtained using the same selection cuts in all charged-particle species. To visualize better, we multiplied scale factors to each p_T spectrum. From the lower panel of Fig. 3, the p_T spectrum corresponding to (30–40)% centrality is seen to coincide with the MB spectra. For the threshold centrality class (30–40)%, classes (0–5)%, (5–10)%, (10–20)%, and (20–30)% are harder while classes (40–50)%, (50–60)%, (60–70)%, and (70-80)% are softer with respect to MB. It is to be noted that a similar trend is observed for all the identified particles. We report a shift in the hardness of the p_T spectra from most central to peripheral collisions. The ratios change from low p_T to high p_T and this change is ≈5% down to ≈20% for 0–5% and 70–80% central events respectively. This is due to the loss of hard processes

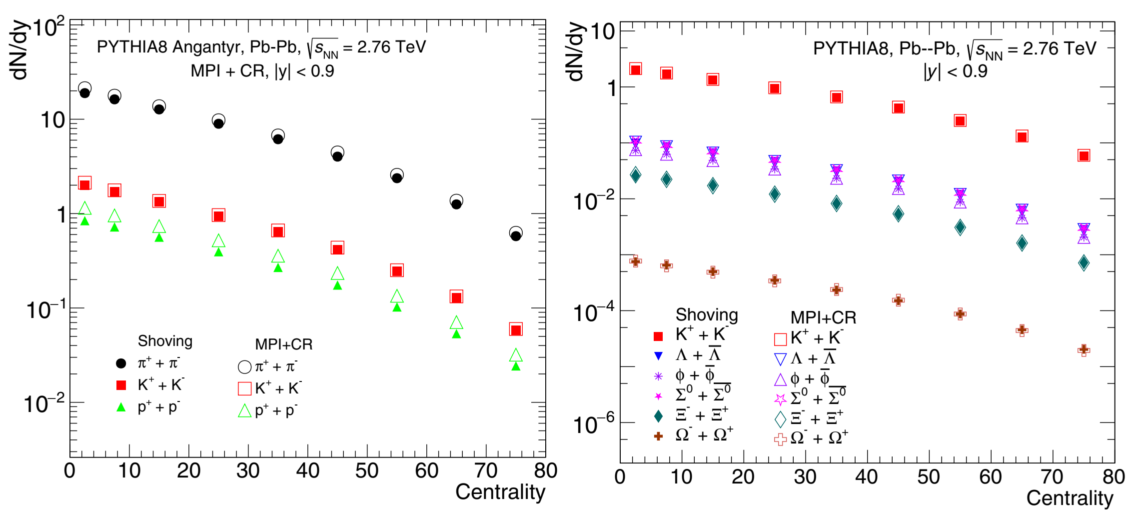

FIG. 7. Yield of identified particles (left) and strange particles (right) as a function of centrality with MPI+CR and string shoving.

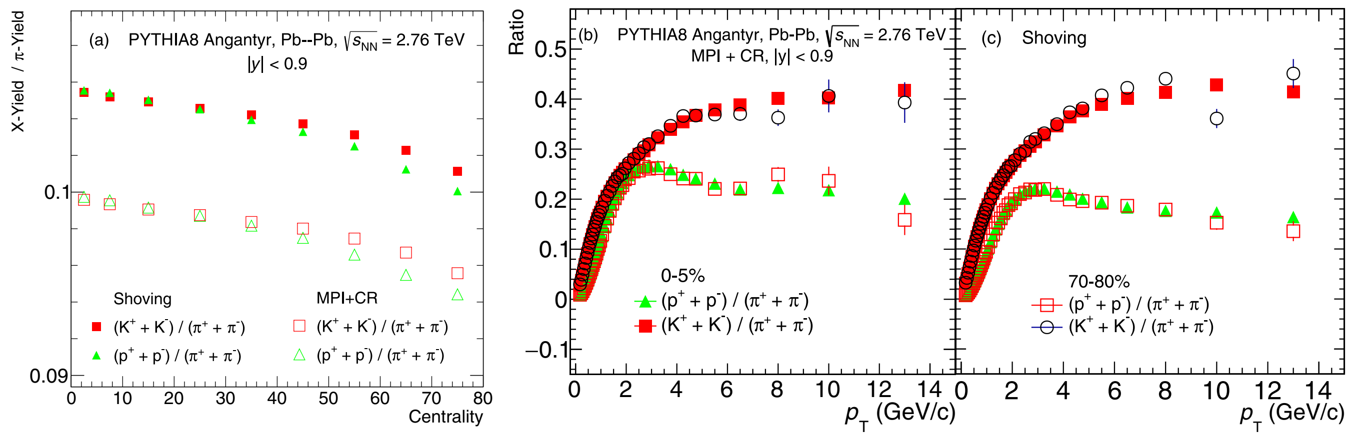

FIG. 8. Ratio of yields of identified particles over $\pi^+ + \pi^-$ as a function of centrality (a) and as a function of transverse momentum with (b) MPI+CR and (c) string shoving.

in peripheral collisions, which is reflected in high p_T particle production.

The p_T spectra of hadrons obtained at the final state are compared to measurements from the ALICE. In Fig. 4 the PYTHIA predictions find a good match with the data for pions, kaons, and protons; however, an underestimation at low p_T is observed. The hump at low p_T is probably due to the perturbative QCD (pQCD) implementation of PYTHIA, whereas we expect nonrelativistic QCD (NRQCD) effects in this regime. The effects of radial flow and other medium effects are contributing factors, which can explain the bump at low p_T as reported in [40,41]. We also compare strange baryon p_T spectra (Λ, Ξ, Ω) with ALICE in all centrality ranges considered, as shown in Fig. 5. The ratios show a similar peak at $p_T \approx 3$ GeV/c. It is also observed that the width of the hump increases with strangeness and mass, especially for central and semicentral events. At higher centralities, the strange baryons show good compatibility. In Fig. 6, we compare the ϕ meson and D meson (D^0, D^+) p_T spectra, where the ϕ meson spectra are seen to be consistent with ALICE measurements in all centralities. As ϕ mesons decay outside a produced fireball, medium effects do not affect the production process [42]. A thermalized QGP state is not a part of PYTHIA8 Angantyr, which may result in a good description of experimental results. In the case of D mesons, we see PYTHIA predictions depart at low p_T; however, the are in good agreement at intermediate-higher values. This helps us to conclude that the more prominent peaks observed for strange baryons (Fig. 5) have a strangeness rather than mass dependence. In a comparison between the tunes, there is no noticeable difference between the results from MPI+CR and string shoving, showing identical ratios for data over model calculations for all aforementioned species, except Ξ. The p_T spectra for Ξ from string shoving describe the experimental measurements better than the MPI+CR tune.

B. p_T integrated yield of identified and strange particles

The p_T integrated yields of $\pi^{\pm}$, $K^{\pm}$, and $p(\bar{p})$ are shown in Fig. 7 (left) within rapidity range $-0.9 < y < 0.9$ normalized by the total number of events. It is observed that the yields of different particles are increasing going from peripheral to most central. We can see a clear mass ordering in yields, with lower mass pions having higher yields, while protons,

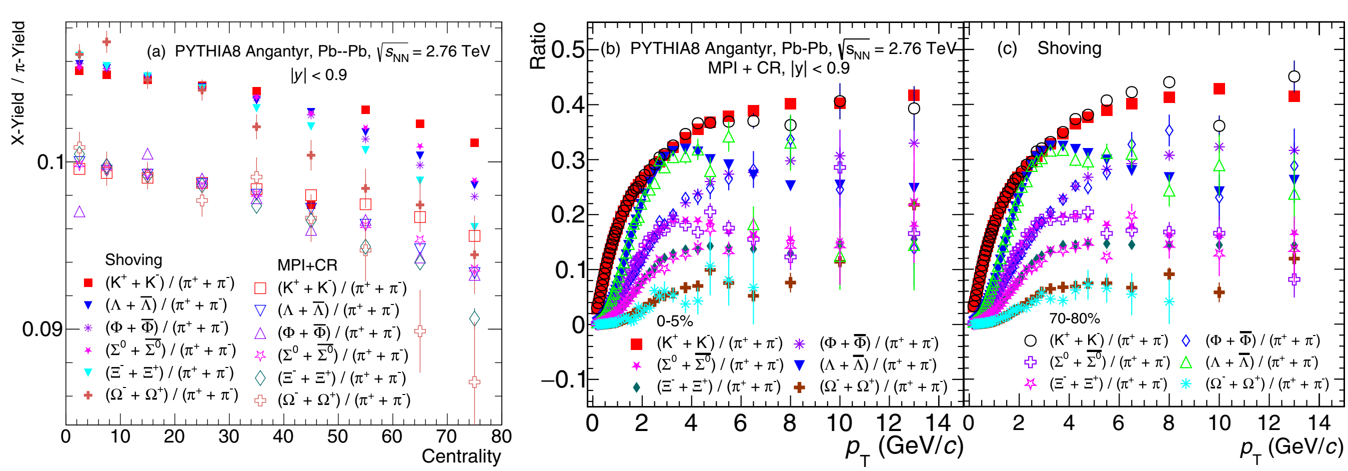

FIG. 9. Ratio of yields of strange particles over $\pi^+ + \pi^-$ as a function of centrality in (a) and as a function of transverse momentum with (b) MPI+CR and (c) string shoving.

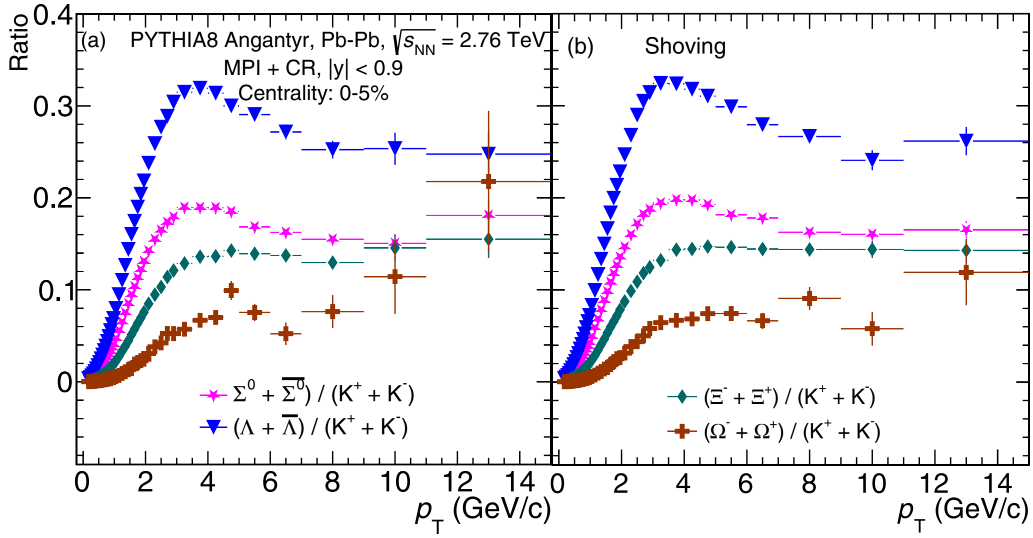

FIG. 10. Ratio of yields of strange particles over $(K^+ + K^-)$ as a function of transverse momentum with (a) MPI+CR and (b) string shoving included.

being heavier, have lower yields. This is expected towards central collisions; the probability for hard scatterings will be higher, resulting in high particle production. Production of a lighter particle requires less energy compared to a heavier particle and will be more dominant in peripheral collisions. The PYTHIA8 Angantyr configurations show minor deviations in proton and π yields, with a slightly higher yield in Angantyr.

In Fig. 7 (right), p_T integrated yields of strange particles are shown. One can see the same features in strange particles like that of identified particles observed in Fig. 7 (left). Production of strange particles is seen to reduce towards peripheral collisions with a similar trend in mass, except for ϕ mesons.

C. Particle ratios

By the bare yield distribution, we cannot quantitatively measure the enhancement or suppression of different particle species. The best way to do this is to estimate the yield with respect to other particles. We measure the ratio of proton and kaon yields over pions to inspect the variation over centrality and p_T. Figure 8 shows the measured yield ratios vs centrality (a) and p_T [(b) and (c)]. We scale proton over pion ratios for every centrality class for better comparison with the corresponding quantity versus p_T (a). The scale factor is calculated using the formula

$$\text{scale factor} = \frac{K/\pi}{X/\pi}.$$

Here X refers to different particle species. We can see from Fig. 8 that both ratios are increasing towards most central; however, the proton over pion (p/π) ratio drops more rapidly than kaon over pion (K/π). There is a visible deviation of $\approx$5% between MPI+CR and string shoving. The reason could be slight overestimation of π and proton yields for MPI+CR compared to string shoving. As a function of p_T, K/π ratio increases at lower p_T but decreases at higher p_T, showing a bump around 3 GeV/c. In heavy-ion collisions, this is the consequence of radial flow, but in PYTHIA, this is attributed to the string interactions in color reconnection or string shoving. We can argue that CR or string shoving could be another mechanism of flow where a longitudinal boost is implemented at the initial state (partonic state), prior to hadronization. Understanding this mechanism is important, as it can provide an explanation of flowlike patterns in PYTHIA. At higher p_T, more particles correspond to jets, in which these particles become insensitive to the hadronization mechanism. If one increases MPI, we see an enhancement in the bump region. In contrast to experimental measurements [43], we do not observe any bump in the K/π ratio. A similar behavior is seen for meson to pion ratios. For baryon to pion ratios, however, the bump is seen to shift further in p_T with increasing mass. The results are shown for both the tunes, showing close similarity between the results. This is a qualitative attempt with PYTHIA8 Angantyr to describe meson and baryon over meson ratios. Studies report this effect can also be observed in meson to meson ratios with further tuning. [36]. Similarly, we show yield ratios of strange particles over pions as a function of centrality in Fig. 9(a). Each yield ratio of different particles is scaled with a similar method as mentioned before. A $\approx$5% deviation between the tunes is seen here due to the slightly higher π yields. We observe a clear strangeness enhancement as we go from most central to peripheral collisions. Heavy strange particle ratios are showing more enhancement, as reported in Fig. 9(a); slopes of strange particle ratios increase towards heavier strange particles. This is due to overlapping color strings forming (ropes) at higher densities [29]. In Fig. 9, we show yield ratios of strange particles as a function of transverse momentum in two different centrality classes, 0–5% and 70–80%. For all strange particles, yield ratios increase towards higher p_T. As expected, the ratio of yields is lower for strange heavy particles. We also conclude by observing in Figs. 8 (right) and 9 (right) that meson to pion ratios are not showing the bump, but a bump shows for baryon to pion ratios.

In Fig. 10 we show the ratio of strange particles over $(K^+ + K^-)$ mesons. The ratio increases as p_T increases, and after a peak close to 3–4 GeV/c, it decreases. The position of the peak shifts towards higher p_T for strange heavy particles. A study reports a similar type of observation seen in experimental data for Pb-Pb collisions [44]. This effect is generally seen in heavy-ion collisions as a consequence of radial flow [45].

IV. SUMMARY

In this work, we attempt to study the dynamics of particle production in Pb-Pb collisions at $\sqrt{s_{NN}} = 2.76$ TeV using the Angantyr model incorporated in PYTHIA8. This model is an extrapolation of pp collision into pA and AA collisions without a thermalized medium. Without any collectivity present, we report that MPI with CR and string shoving mimic flowlike features [46]. In this regard, the primary observations of this work are summarized below:

(i) The multiplicity distribution of charged particles with different combinations, namely MPI+CR and string shoving tunes, are compared to ALICE measurements. It is observed that, setting CR off, PYTHIA8 Angantyr predictions overestimate ALICE data, whereas turning MPI off underestimates the data. The MPI+CR setting is observed to be a good tune to match the multiplicity distribution obtained from PYTHIA with ALICE results. String shoving is seen to describe the experimental results better than MPI+CR.

(ii) The p_T spectra of charged-particles simulated by PYTHIA8 Angantyr at different centralities are also consistent with experimental data at intermediate and high p_T. It is also observed that the $\langle p_T \rangle$ distribution obtained by using MPI + CR is consistent with ALICE data. The results from string shoving are fairly compatible with MP+CR and no visible difference is observed.

(iii) p_T spectra of identified particles [$\pi^\pm$, $K^\pm$, $p(\bar{p})$] in different centrality classes along with minimum bias (MB) aerre obtained. Hardening of the p_T spectra can be seen towards most central collisions and is more pronounced for heavier particles. A centrality cutoff at (30–40)% is observed and found to coincide with MB, which implies centralities above this cutoff produce harder particles.

(iv) The p_T integrated yield normalized by total events of identified charged particles and strange particles show a clear mass ordering. Heavier particle production is lower and decreases towards peripheral collisions. The rate of production with respect to pions is higher for protons compared to kaons towards central collisions

(v) It is observed that the ratio of kaon over pion as a function of p_T increases with increasing p_T and then saturates toward higher p_T. This measurement is, however, incompatible with experimental results from ALICE, which show a prominent peak at low p_T. In contrast, the ratio of proton over pion shows a peak around 3 GeV/c due to CR with MPI and string shoving in PYTHIA8, which mimic flo-like patterns. A similar rise is observed for all the strange baryon over pion ratios, although it is unobserved for the meson to meson ratio. The mass dependence of the shift in the peak with p_T is reproduced well by the model.

(vi) It is observed that the slope of the strange particles to pion ratio as a function of centrality is more significant for strange heavy particles. We report that the peak of the strange baryon to pion ratio and of strange baryon to kaon as a function of p_T shifts toward higher p_T for heavier strange particles. This shows that strangeness enhancement is dominant in strange heavy particles, which is a consequence of color strings overlapping at higher densities in accordance with the CR and string shoving.

From the present study and the subsequent observations, it can be concluded that PYTHIA8 Angantyr provides tunes favorable to study observables relevant in heavy-ion collisions. In Angantyr, MPI with CR as well as string shoving configuration provide testable results. The model, however, fails in the low p_T regime, when compared to the measurements from ALICE. The transverse momentum bump at low p_T due to radial flow relates to the absence of a thermalized medium in PYTHIA8 Angantyr; in contrast it is well established by hydrodynamic models. Further tuning in PYTHIA8 Angantyr modes may lead to a better description of the bump region. Both tunes mimic flowlike features as seen from the baryon over meson ratios as a function of p_T. The baryon over meson ratios describe the peaks qualitatively; however, the meson over meson results deviate from the experimental measurements. The strength of collectivity mimicking effects may also be the cause of dissimilarity between the model and data. Although we have shown features resembling radial flow, one can also observe higher-order flow harmonics (v_2, v_3) in models that pertain to QGP free collision systems [47].

ACKNOWLEDGMENTS

R.S. acknowledges financial support (DST/INSPIRE Fellowship/2017/IF170675) by the DST-INSPIRE program of the Government of India. R.S. is also grateful to the authors of PYTHIA8 and PYTHIA8 Angantyr.

[1] F. Gao and J. M. Pawlowski, Phys. Rev. D **102**, 034027 (2020).
[2] A. N. Tawfik, Indian J. Phys. **91**, 93 (2017).
[3] H. Satz, Int. J. Mod. Phys. A **28**, 1330043 (2013).
[4] W. Busza, K. Rajagopal, and W. van der Schee, Annu. Rev. Nucl. Part. Sci. **68**, 339 (2018).
[5] D. Teaney, J. Lauret, and E. V. Shuryak, Phys. Rev. Lett. **86**, 4783 (2001).

[6] W. Cassing and E. L. Bratkovskaya, Phys. Rep. **308**, 65 (1999).
[7] B. B. Back *et al.* (PHOBOS Collaboration), Nucl. Phys. A **757**, 28 (2005).
[8] F. Becattini, J. Phys.: Conf. Ser. **527**, 012012 (2014).
[9] Y. Aoki, G. Endrodi, Z. Fodor, S. D. Katz, and K. K. Szabo, Nature (London) **443**, 675 (2006).
[10] R. E. Ansorge *et al.* (UA5 Collaboration), Z. Phys. C **43**, 357 (1989).
[11] C. Albajar *et al.* (UA1 Collaboration), Nucl. Phys. B **335**, 261 (1990).
[12] G. J. Alner *et al.* (UA5 Collaboration), Z. Phys. C **33**, 1 (1986).
[13] G. Arnison *et al.* (UA1 Collaboration), Phys. Lett. B **118**, 167 (1982).
[14] M. L. Miller, K. Reygers, S. J. Sanders, and P. Steinberg, Annu. Rev. Nucl. Part. Sci. **57**, 205 (2007).
[15] K. Adcox *et al.* (PHENIX Collaboration), Nucl. Phys. A **757**, 184 (2005).
[16] P. Braun-Munzinger, K. Redlich, and J. Stachel, in *Quark-Gluon Plasma 3*, edited by R. C. Hwa and X.-N. Wang (World Scientific, Singapore, 2004), pp. 491–599.
[17] F.-H. Liu, Y.-H. Chen, H.-R. Wei, and B.-C. Li, Adv. High Energy Phys. **2013**, 965735 (2013).
[18] J. Cleymans and D. Worku, Eur. Phys. J. A **48**, 160 (2012).
[19] J. Cleymans and D. Worku, J. Phys. G **39**, 025006 (2012).
[20] P. Koch, B. Muller, and J. Rafelski, Phys. Rep. **142**, 167 (1986).
[21] S. Soff, S. A. Bass, M. Bleicher, L. Bravina, M. Gorenstein, E. Zabrodin, H. Stoecker, and W. Greiner, Phys. Lett. B **471**, 89 (1999).
[22] A. Capella, Phys. Lett. B **364**, 175 (1995).
[23] E. Cuautle and G. Paić arXiv:1608.02101.
[24] G. Torrieri, J. Phys. G **36**, 064007 (2009).
[25] J. Adam *et al.* (ALICE Collaboration), Nat. Phys. **13**, 535 (2017).
[26] P. Huovinen, P. F. Kolb, U. W. Heinz, P. V. Ruuskanen, and S. A. Voloshin, Phys. Lett. B **503**, 58 (2001).
[27] K. Aamodt *et al.* (ALICE Collaboration), Phys. Rev. Lett. **105**, 252302 (2010).
[28] J. Adams *et al.* (STAR Collaboration), Phys. Rev. C **72**, 014904 (2005).
[29] C. Bierlich, G. Gustafson, L. Lönnblad, and H. Shah, J. High Energy Phys. 10 (2018) 134.
[30] T. Sjostrand, S. Mrenna, and P. Z. Skands, J. High Energy Phys. 05 (2006) 026.
[31] T. Sjostrand, S. Mrenna, and P. Z. Skands, Comput. Phys. Commun. **178**, 852 (2008).
[32] S. G. Weber, A. Dubla, A. Andronic, and A. Morsch, Eur. Phys. J. C **79**, 36 (2019).
[33] J. P. Lees *et al.* (BaBar Collaboration), Phys. Rev. D **92**, 072015 (2015).
[34] M. Martinez, Nucl. Phys. A **926**, 242 (2014).
[35] B. Andersson, S. Mohanty, and F. Soderberg, Eur. Phys. J. C **21**, 631 (2001).
[36] A. Ortiz Velasquez, P. Christiansen, E. Cuautle Flores, I. A. Maldonado Cervantes, and G. Paić, Phys. Rev. Lett. **111**, 042001 (2013).
[37] N. K. Behera, R. K. Nayak, and S. Dash, Phys. Rev. C **101**, 064903 (2020).
[38] B. B. Abelev *et al.* (ALICE Collaboration), Phys. Lett. B **727**, 371 (2013).
[39] B. Abelev *et al.* (ALICE Collaboration), Phys. Lett. B **720**, 52 (2013).
[40] X. Zhu, F. Meng, H. Song, and Y. X. Liu, Phys. Rev. C **91**, 034904 (2015).
[41] K. Werner, I. Karpenko, M. Bleicher, T. Pierog, and S. Porteboeuf-Houssais, Phys. Rev. C **85**, 064907 (2012).
[42] M. Nasim, V. Bairathi, M. K. Sharma, B. Mohanty, and A. Bhasin, Adv. High Energy Phys. **2015**, 197930 (2015).
[43] B. B. Abelev *et al.* (ALICE Collaboration), Phys. Lett. B **736**, 196 (2014).
[44] B. B. Abelev *et al.* (ALICE Collaboration), Phys. Rev. Lett. **111**, 222301 (2013).
[45] R. J. Fries and B. Muller, Eur. Phys. J. C **34**, s279 (2004).
[46] I. A. Maldonado-Cervantes, E. Cuautle, G. Paic, A. Ortiz Velasquez, and P. Christiansen, J. Phys.: Conf. Ser. **509**, 012064 (2014).
[47] A. V. da Silva, W. M. Serenone, D. Dobrigkeit Chinellato, J. Takahashi, and C. Bierlich, arXiv:2002.10236.